Delocalization in electron-impact ionization in a crystalline environment

L. J. Allen
School of Physics, University of Melbourne, Parkville, Victoria 3052, Australia

C. J. Rossouw
Division of Materials Science and Technology, Commonwealth Scientific and Industrial Research Organization, Locked Bag 33, Clayton, Victoria 3168, Australia

(Received 24 April 1992; revised manuscript received 18 September 1992)

A theory for variations in cross section with diffraction conditions for electron-impact ionization of atoms in a crystalline environment is presented. This takes into account total interaction delocalization (due both to long-range Coulombic interaction and thermal smearing of the target position) by integration over all scattering angles and ejected electron momenta as well as attenuation of dynamical effects by inelastic scattering, particularly thermal diffuse scattering. These results are of fundamental importance for atom location by channeling-enhanced microanalysis using energy-dispersive x-ray or electron-energy-loss-spectroscopy techniques. Agreement between this theory and various energy-dispersive x-ray experiments reported in the literature (as well as our own experiments) under dynamical electron-diffraction conditions is satisfactory.

I. INTRODUCTION

In this paper we present an expression for atomic ionization cross sections in a crystalline environment under dynamical electron diffraction conditions. This incorporates ionization kinematics and associated delocalization from first principles, with proper integration over all final states of the scattered fast electron as well as the ejected target electron. This theory also accounts for ionization from dechanneled electrons (such as those which have been thermally scattered) as well as delocalization due to thermal fluctuations in target atom position. This formulation, which extends previous work[1] which did not explicitly incorporate inelastic scattering into the ionization cross section, is of fundamental importance for ionization probabilities measured under strong diffraction conditions by electron energy loss spectroscopy (EELS) or energy dispersive x-ray (EDX) spectroscopy as well as for interpretation of results from the associated technique of atom location by channeling-enhanced microanalysis (ALCHEMI).[2,3] Various methods to include localization effects in ALCHEMI have been suggested[4–9] but none of these is of general applicability.

The validity of this theory is tested by correlation with EDX spectra recorded under various dynamical diffraction conditions. We use a modified hydrogenic model for the atomic electron which is adequate for K-shell excitation and which is computationally convenient.[3,10,11] However it should be noted that the theory is in principle not limited to this particular model for the $(e,2e)$ transition matrix elements.

II. THEORY

The dynamical equations of Bethe[12] are a starting point for a general theory of electron diffraction in a crystal:

$$[\mathbf{K}^2-(\mathbf{k}^i+\mathbf{g})^2]C_g^i+\sum_{h\neq g}U_{g-h}C_h^i=0\ . \tag{1}$$

There is one equation for each Bloch wave on branch i of the dispersion surface. $K^2=k^2+U_0$, where $\mathbf{k}$ is the vacuum wave vector of the fast electron and U_0 is related to the mean inner crystal potential. Inelastic scattering is treated by an absorptive potential, by including an imaginary component in the Fourier coefficients U_{g-h}. The most important inelastic effect contributing to anomalous absorption is due to thermal diffuse scattering (TDS).[13–15] Other delocalized electronic excitations (plasmons, single electron excitations) can be accounted for by inclusion of an extra mean absorptive term. Small angle scattering processes such as plasmon excitations generally preserve diffraction contrast and channeling phenomena. However, even for low energy losses, scattering through more than a Bragg angle contributes to a dechanneled component that by integration over all angles adds a plane wave background component to channeling and associated inelastic phenomena.

The boundary conditions at the crystal surface allow us to express each $\mathbf{k}^i$ in the form[13]

$$\mathbf{k}^i=\mathbf{K}+\lambda^i\hat{\mathbf{n}}=\mathbf{K}+(\gamma^i+i\eta^i)\hat{\mathbf{n}}\ , \tag{2}$$

where we explicitly decompose the complex eigenvalue into its real part γ^i (the *anpassung)* and imaginary part η^i (the absorption coefficient). $\hat{\mathbf{n}}$ is a unit vector in the direction of the surface normal, directed into the crystal. The Bloch wave expansion for the wave function in the crystal is given by

$$\psi(\mathbf{K},\mathbf{r})=\sum_i A^i\sum_g C_g^i\exp[i(\mathbf{K}+\lambda^i\hat{\mathbf{n}}+\mathbf{g})\cdot\mathbf{r}]\ . \tag{3}$$

The presence of an imaginary component $U''(\mathbf{r})$ in the potential (representing absorption due to ionization in our case) in the Schrödinger equation can readily be shown[16] to give rise to a rate of loss of electrons per unit volume at the point $\mathbf{r}$ (due to ionization) proportional to the quantity $P=\psi\psi^*(\mathbf{r})U''(\mathbf{r})$. We follow the theoretical approach outlined by Cherns, *et al.*[17] and integrate P

over the volume of the crystal using the expressions given for $\psi\psi^*$ in Ref. 13 (including absorption due to all inelastic processes) and that for the ionization potential given in Ref. 1 in such a way that these two quantities are correctly convoluted together. This generalizes the expression for the ionization cross section in Ref. 1 to take into account the effect of other inelastic background scattering on the ionization cross section. The result can also be obtained along the lines of the lengthy derivation in Ref. 18 by including absorption in the relevant Bloch waves at the outset. The result for the cross section for ionization in the presence of other background inelastic scattering is of the form

$$\sigma = NV_c \left[\left[1 - \sum_{ij} B(i,j,t) S(i,j) \right] \mu_0 + \sum_{ij} B(i,j,t) \sum_{gh} C_g^i C_h^{j*} \mu_{h-g} \right] , \tag{4}$$

where N is the number of unit cells in the crystal and V_c is the unit cell volume. The term $B(i,j,t)$ relates to the Bloch wave amplitudes A^i, real part of the eigenvalues γ^i and absorption coefficients η^i of each partial wave from which the total wave function in the crystal is reconstructed, and is given by

$$B(i,j,t) = A^i A^{j*} \frac{\eta_z^i + \eta_z^j + i(\gamma_z^i - \gamma_z^j)}{(\eta_z^i + \eta_z^j)^2 + (\gamma_z^i - \gamma_z^j)^2} \frac{\{1 - \exp[-(\eta_z^i + \eta_z^j)t] \exp[i(\gamma_z^i - \gamma_z^j)t]\}}{t} . \tag{5}$$

where t is the crystal thickness, $\gamma_z^i = \gamma^i \hat{\mathbf{n}} \cdot \hat{\mathbf{z}}$ where $\hat{\mathbf{z}}$ is along the crystallographic z direction and η_z^i is similarly defined. The term $S(i,j)$ is given in terms of the components of the eigenvectors by

$$S(i,j) = \sum_g C_g^i C_g^{j*} \tag{6}$$

and this term is unity for normal incidence. The term μ_{h-g} (with μ_0 a special case) is of the form

$$\mu_{h-g} = \frac{4n}{(2\pi)^3 k a_0^{*2} V_c} \mathcal{F}[\text{site}] \mathcal{F}[\text{kin}] , \tag{7}$$

where the factor n is inserted to account for the number of electrons in the initial target shell, a_0^* is the relativistic Bohr radius and V_c is the unit cell volume.

The site dependent term

$$\mathcal{F}[\text{site}] = \sum_{\beta n} \exp[-M(\mathbf{g}-\mathbf{h})] \exp[i(\mathbf{g}-\mathbf{h}) \cdot \tau_{\beta n}] \tag{8}$$

where $\tau_{\beta n}$ are the n sites of atom type β in the unit cell and the Debye-Waller factor $M(\mathbf{q}) = \frac{1}{2} q^2 \langle u_\beta^2 \rangle$, where $\langle u_\beta^2 \rangle$ is the mean-square atomic displacement. The exponential factor containing the Debye-Waller factor has been inserted in Eq. (8), following Ref. 17, to take into account the broadening of the ionization potential at each atomic site due to the thermal vibrations of the target atom. The atomic positions are convoluted in real space with the Debye-Waller factor obtained within the context of an Einstein model for TDS, leading to a multiplicative term in Eq. (8) to take into account the uncertainty in absolute position due to the thermal motion. In practice the inclusion of this term was found to make negligible difference to the cross sections since the ionization remains localized relative to the dynamical fast electron wave function. To a good approximation ionization can be considered as occurring independently against a mean attenuation due to fast electrons which have been dechanneled due to electronic excitation plus a thermally generated component, as one would expect with the ionization potential being much less than that due to TDS—a quantitative comparison between these two potentials is made in the next section.

The interaction kinematics term

$$\mathcal{F}[\text{kin}] = \int_0^{\kappa_{\max}} k' \kappa^2 \left[\int \frac{1}{Q_g^2 Q_h^2} \left[\int F(\mathbf{Q}_g, \boldsymbol{\kappa}) F^*(\mathbf{Q}_h, \boldsymbol{\kappa}) d\Omega_\kappa \right] d\Omega \right] d\boldsymbol{\kappa} \tag{9}$$

with $\mathbf{Q}_g = \mathbf{q} + \mathbf{g}$ and $\mathbf{Q}_h = \mathbf{q} + \mathbf{h}$, where the momentum transfer $\mathbf{q}$ is given in terms of the incident and scattered wave vectors $\mathbf{k}$ and $\mathbf{k}'$ by $\mathbf{q} = \mathbf{k} - \mathbf{k}'$. Analytic expressions[10,11] have been given (assuming a hydrogenlike model for ionization) for the quantity

$$\int F(\mathbf{Q}_g, \boldsymbol{\kappa}) F^*(\mathbf{Q}_h, \boldsymbol{\kappa}) d\Omega_\kappa , \tag{10}$$

where, if $\mathbf{Q}_g \neq \mathbf{Q}_h$, these "nondiagonal" terms contribute to the site-sensitivity and orientation dependence of the ionization cross section. The accuracy of the hydrogenic model, at least for diagonal terms, is considered in Ref. 3 as a function of the nuclear charge and energy of the incident electron and is expected to be reasonable for the elements and energies considered here. More particularly, in Eq. (10) we have

$$F(\mathbf{q}, \boldsymbol{\kappa}) = \int u_f^*(\boldsymbol{\kappa}, \mathbf{r}') \exp(i\mathbf{q} \cdot \mathbf{r}') u_i(\mathbf{r}') d\mathbf{r}' , \tag{11}$$

where $u_i(\mathbf{r}')$ and $u_f(\boldsymbol{\kappa}, \mathbf{r}')$ are the initial and final state wave functions of the target electron, $u_f(\boldsymbol{\kappa}, \mathbf{r}')$ representing a continuum final state with $\boldsymbol{\kappa}$ the ejected electron wave vector. For a particular ejected electron wave vector $\boldsymbol{\kappa}$ and for each element $\mathbf{Q}_g$, $\mathbf{Q}_h$ and $d\Omega$, integration of Ω_κ over all ejection directions is evaluated from Eq. (10).

The second integral in Eq. (9) is numerically integrated over 4π steradians for the scattered electron wave vector $\mathbf{k}'$. The first integral is then evaluated with κ being incremented by $\Delta\kappa$, and numerical integration over Ω and Ω_κ repeated. Thus the $(e,2e)$ cross section for ionization is integrated over all target electron momenta $\boldsymbol{\kappa}$, all scattered electron momenta $\mathbf{k}'$ and all ejection energies above threshold (equivalent to integrating over κ).

The first term in Eq. (4), the factor in large parentheses times μ_0, takes into account the contribution from dechanneled fast electrons to ionization. Explicitly the term μ_0 in Eq. (4) is given by

$$\mu_0=\frac{4nn_\beta}{(2\pi)^3 k a_0^{*2} V_c}\int_0^{\kappa_{\max}} k'\kappa^2\left[\int\frac{1}{q^4}\left[\int F(\mathbf{q},\boldsymbol{\kappa})F^*(\mathbf{q},\boldsymbol{\kappa})d\Omega_\kappa\right]d\Omega\right]d\kappa\ . \tag{12}$$

For kinematic conditions ($\mathbf{Q}_g=\mathbf{Q}_h=\mathbf{q}$), Eq. (4) reduces to

$$\sigma=NV_c\mu_0=N\frac{V_c}{\lambda_0}=Nn_\beta\left[\frac{V_c}{n_\beta\lambda_0}\right]=Nn_\beta\left[\frac{1}{n_0\lambda_0}\right], \tag{13}$$

where $\lambda_0=1/\mu_0$ is the kinematic mean free path for ionization, n_β is the number of atoms of type β in a unit cell and $n_0=n_\beta/V_c$ (i.e., under these conditions the total cross section is the cross section for an isolated atom multiplied by the number of atoms). This result is also achieved in the limit as the crystal thickness $t\to\infty$, i.e., we obtain Eq. (13) but this time from the first term in Eq. (4). Thus the asymptotic behavior of Eq. (4) is reasonable: for kinematic diffraction conditions or for thick specimens the cross section is the sum of isolated atomic cross sections.

With the assumption that

$$\mu_{h-g}n_\beta\approx\mu_0\mathcal{F}[\text{kin}] \tag{14}$$

for all $\mathbf{h}-\mathbf{g}$, Eq. (4) reduces to

$$\sigma=\frac{NV_c}{n_\beta\lambda_0}\left[n_\beta\left[1-\sum_{ij}B(i,j,t)S(i,j)\right]+\sum_{ij}B(i,j,t)\sum_{gh}C_g^iC_h^{j*}\mathcal{F}[\text{site}]\right]. \tag{15}$$

Setting the exponential term containing the Debye-Waller factor to unity in Eq. (8), Eq. (15) can be rewritten in terms of the inelastically attenuated probability density $\psi\psi^*$ on the n atoms of type β (see Ref. 13) as

$$\sigma=\frac{NV_c}{n_\beta\lambda_0}\psi\psi^*_{av}\ . \tag{16}$$

This result represents a many-beam generalization of the expression of Cherns *et al.*[17] for the cross section attenuated by thermal absorption (plus a mean absorption due to other inelastic processes where this is important) for characteristic x-ray emission under dynamical diffraction conditions. The approximation given by Eq. (14) changes the ionization potential to a δ function: thus the isolated atomic cross section in Eq. (13) is multiplied by the thickness-averaged dynamical probability density on these sites.

It should be noted[1] that the Fourier coefficients of the ionization potential are related to the μ_{h-g} as follows:

$$U''_{h-g}=\frac{k}{(2\pi)^2}\mu_{h-g}\ . \tag{17}$$

Thus the ionization cross section σ may be explicitly written in terms of Fourier components of the ionization potential, coupled with eigenvalues and eigenvectors and absorption coefficients due to TDS plus a possible mean absorption due to delocalized electronic processes.

III. RESULTS

A 2D projection of the elastic crystal potential $V_{\text{El}}(\mathbf{r})$ and TDS potential $V_{\text{TDS}}(\mathbf{r})$ for the ⟨110⟩ zone axis of GaAs (300 K and 300 keV beam) is plotted in Fig. 1(a) and 1(b), each constructed from a two-dimensional array of more than 10^3 Fourier coefficients. Explicit expres-

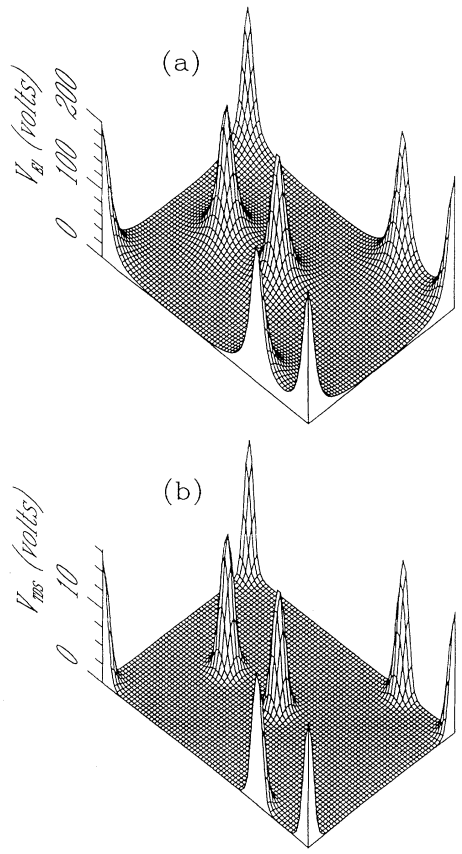

FIG. 1. 2D surface representations of potentials for GaAs viewed down the ⟨110⟩ zone axis, showing (a) V_{El} and (b) V_{TDS}.

sions used for the calculation of V_{TDS} can be found in Ref. 1. Note that V_{TDS} is significantly more localized than V_{EI} on this simple Einstein model.[1] Projected ⟨111⟩ elastic and TDS potentials are shown in Fig. 2(a), V_K for K-shell ionization (with and without thermal smearing) in Fig. 2(b) and V_K is compared with V_{TDS} in Fig. 2(c). The scaling by a constant of the present ionization potentials relative to the corresponding results in Ref. 1 is due to a coding error in those calculations (which does not affect the other results or the conclusions in that paper). At 300 K projected rms displacements $\langle u^2 \rangle^{1/2}$ for Ga and As are 0.090 Å and 0.094 Å (see Reid[19]), resulting in a half-width half-maximum for V_{TDS} of about twice the rms value (0.156 Å for Ga and 0.159 Å for As). These results are slightly different to those in Ref. 1 (where full-width half maxima are given) due to a greater number of Fourier coefficients in the construction of the potential. The shape of $V_K(\mathbf{r})$ is thermally smeared, the intrinsic K-shell excitation half-width half-maxima of 0.033 Å for Ga and 0.028 Å for As being broadened to 0.119 Å and 0.120 Å, respectively.

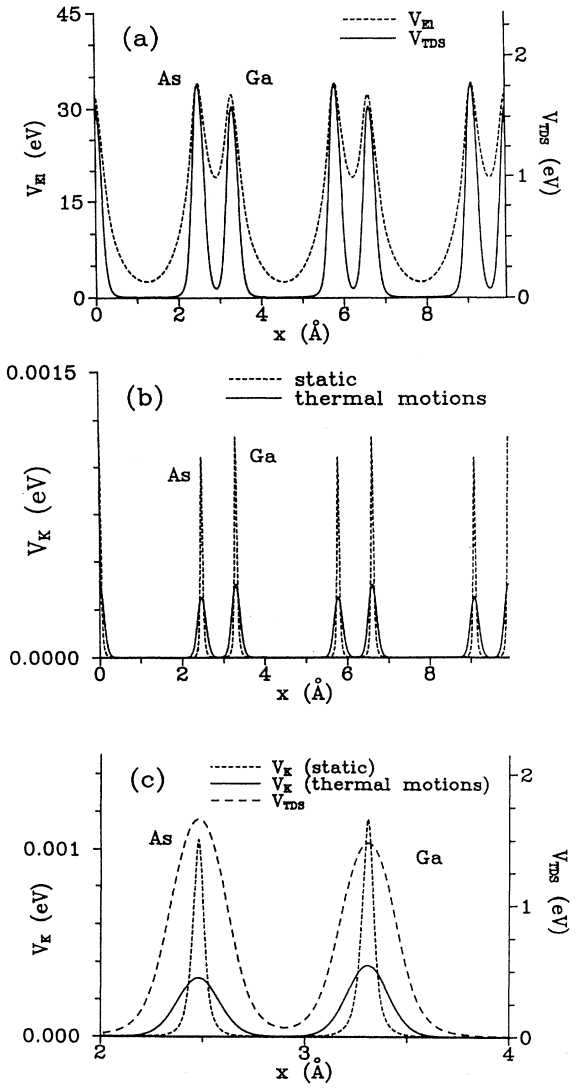

FIG. 2. (a) Projected ⟨111⟩ potentials showing V_{EI} and V_{TDS}. (b) V_K for static atoms and with thermal motions. (c) A comparison of V_{TDS} and V_K from 2 to 4 Å along ⟨111⟩.

We have used the above formalism to calculate ionization cross sections (and hence x-ray emission cross sections and ratios thereof) for various incident beam energies and at 300 K as a function of orientation. We assume K-shell ionization for our calculations [$n=2$ in Eq. (7)] and for which a modified hydrogenic model[3,10,11] is adequate in evaluating the transition matrix elements given by Eq. (11). EDX yields as a function of orientation, the basis of ALCHEMI, have been investigated by a number of authors.[20–24] Figure 3(a) shows the As/Ga K-shell emission ratio from a 2600 Å GaAs specimen at 300 K, subject to various {111} systematic row diffraction conditions with a 300 keV incident beam. Fifteen beams were used in this and the subsequent calculations for GaAs, with dechanneling due to TDS. The x-ray emission cross section for each atom was obtained by scaling the ionization cross section by the appropriate fluorescence yield ω_K (Ref. 25)—this has been done in all subsequent calculations. The theoretical ratio was then scaled by a factor 1.06 to obtain agreement with experiment. Here a total convergence angle of 1.8 mrad and probe size of 25 nm were used, and x-rays detected with a windowless detector on a Philips CM30 microscope. The results accounting for full interaction delocalization are almost indistinguishable from those obtained using the

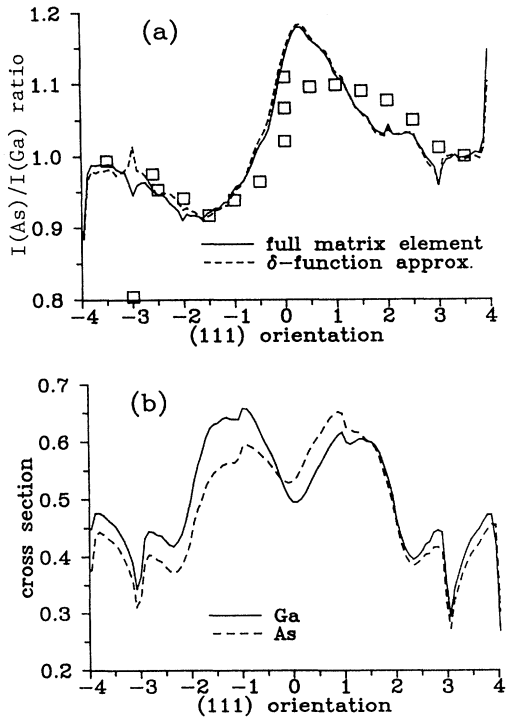

FIG. 3. (a) Correlation of measured As/Ga emission ratios for a {111} systematic row orientation with theory for GaAs, 300 K and 300 keV, thickness 2600 Å. An x-axis value of unity indicates (111) is in the exact Bragg orientation. (b) Variation in the Ga and As K-shell emission cross section with orientation, parameters as in (a).

δ-function approximation for the interaction potential. Absolute variations in x-ray yield can be satisfactorily predicted if beam current and area are known. The results shown in Fig. 3(b) are obtained assuming unit incident intensity per Å^2 and multiplying by 10^4 (equivalent to assuming a cross sectional area of 10 000 Å^2). The theory enables direct measurement of polarity.[21]

Figure 4(a) shows variations in the As/Ga emission ratio with {111} systematic row diffraction condition in GaAs compared with the experimental results of Taftø[21] for 100 keV electrons at 300 K. Reasonable agreement with theory occurs if a thickness of 400 Å is assumed, although Taftø estimated the thickness of the sample to be approximately 500 Å (these ratio results have been scaled by 0.95 to achieve agreement with Tafto). Once again there is excellent agreement between the results obtained using full interaction kinematics and the δ-function approximation. Note the computed progressive change in emission ratio with orientation as thickness is varied in Fig. 4(b). Theoretical results for the underlying changes in emission from Ga and As for a 400 Å crystal is shown in Fig. 4(c), where comparatively slow variations occur as each Brillouin zone boundary is crossed.

Correlation with experimental results for GaAs for a {311} systematic row orientation[21] are shown in Fig. 5(a), where rapid changes are localized near Brillouin zone boundaries. Reasonable agreement with experiment occurs for a thickness of 600 Å (the theoretical ratio has been scaled by 1.06). Figure 5(b) illustrates the rapid diminution in asymmetry across the symmetrical orientation with increasing thickness. Figure 5(c) shows changes in the cross section for x-ray emission from Ga and As

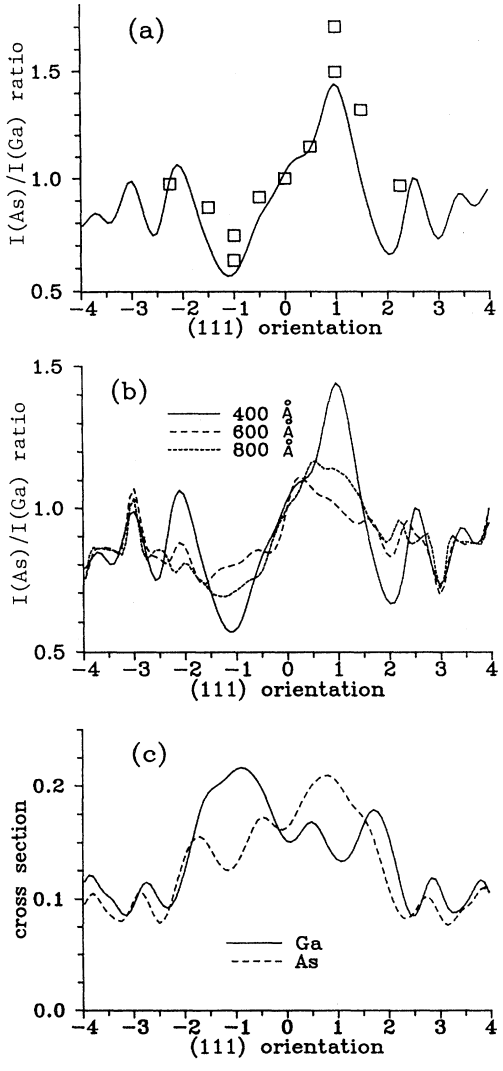

FIG. 4. (a) Correlation of measured As/Ga emission ratios for a {111} systematic row orientation with theory for GaAs, 300 K and 100 keV, thickness 400 Å. (b) Variation in Ga/As emission ratios for thicknesses 400–800 Å. (c) Variation in the Ga and As *K*-shell emission cross sections with orientation (thickness 400 Å).

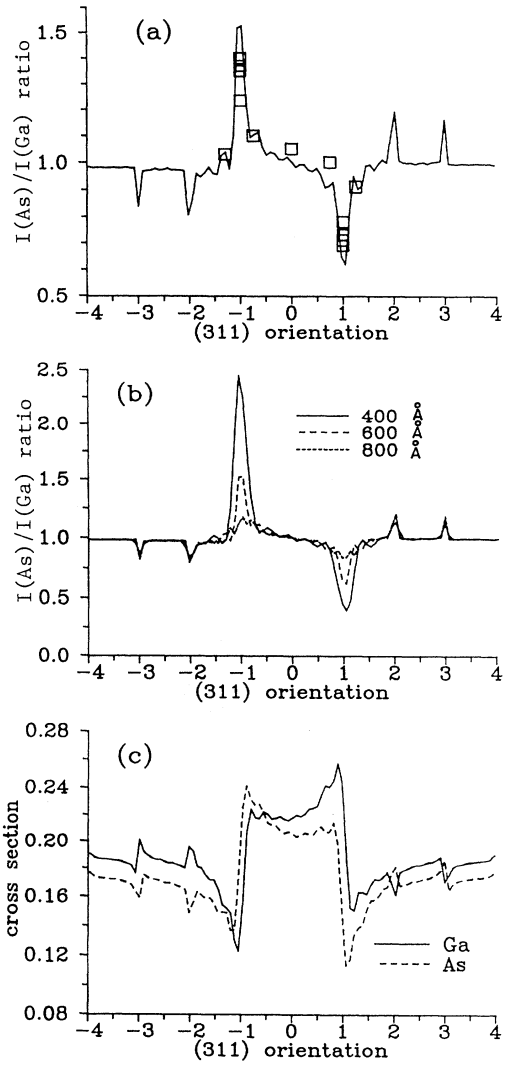

FIG. 5. (a) Correlation of measured As/Ga emission ratios for a {311} systematic row orientation with theory for GaAs, 300 K and 100 keV, thickness 600 Å. (b) Variation in Ga/As emission ratios for thicknesses 400–800 Å. (c) Variation in the Ga and As *K*-shell emission cross section with orientation (thickness 600 Å).

with orientation (thickness 600 Å). In this case rapid variations occur as successive Brillouin zone boundaries are crossed, in contrast with smoother variations in Fig. 4(c) for the {111} systematic row.

Comparison between theory and the experimental results of Taftø[21] for the {200} systematic row of ZnS for 80 keV electrons is shown in Figs. 6(a) (1000 Å thickness, theory scaled by 0.7) and 6(b) (3000 Å thickness, theory unscaled). Nine beams were used in the calculations. Here small but distinct differences occur between the hydrogenic model and a δ-function model due mainly to delocalization associated with *K*-shell excitations for S. Figure 6(c) shows the absolute variations in atomic excitation cross sections for Zn and S using the full hydrogenic model and δ-function model (1000 Å case). For {200} systematic row diffraction conditions the responses are symmetric about the tilt axis.

The results discussed thus far indicate that the δ-function model is a reasonable approximation for the elements involved. Therefore as a further check on the theory outlined here we have taken measurements and done calculations for the lighter element Al, where stronger delocalization effects are expected. In Fig. 7(a) we show results for a {200} systematic row in Al at 300 K. EDX spectra were recorded as a function of orientation from an area measured by convergent beam diffraction contrast to be 3480 Å thick. The difference between the delocalized hydrogenic and δ-function models is clear (nine beams were used in the calculations). Absorption due to TDS as well as (in contrast to previous calculations) a mean absorption (with mean free path 1800 Å) to account for other delocalized inelastic processes is included in the calculations. This was necessary in this case since these effects are important relative to TDS for Al.[26] In Fig. 7(b) theoretical cross sections calculated with no absorption and with absorption due to TDS only are compared with the theoretical curve including both mean absorption and that due to TDS and the experimental results.

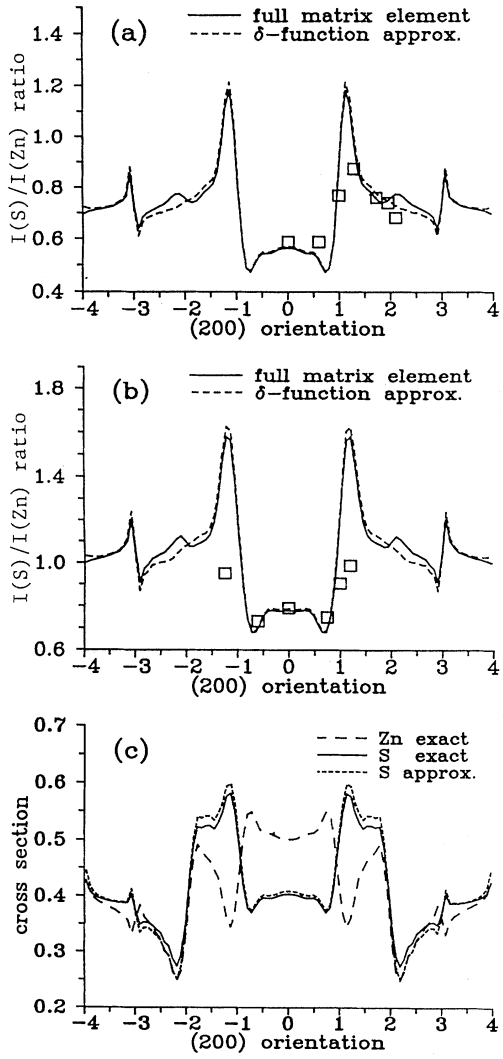

FIG. 6. (a) Correlation of measured S/Zn emission ratios for a {200} systematic row orientation with theory for ZnS, 300 K and 80 keV, thickness 1000 Å. (b) Correlation of S/Zn ratios for a thickness of 3000 Å. (c) Variation in the Zn and S *K*-shell emission cross section with orientation (thickness 1000 Å), showing differences for the hydrogenic model and the δ-function model for *S*.

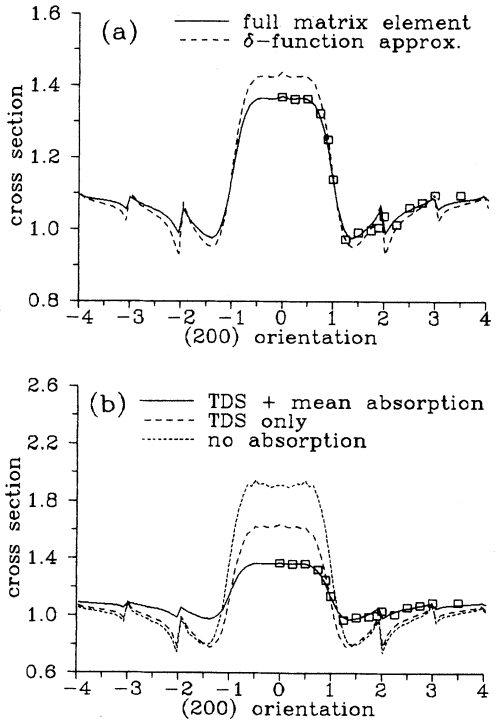

FIG. 7. (a) Correlation of measured x-ray emission cross section for a {200} systematic row orientation with theory for Al, 300 K and 300 keV, thickness 3480 Å. Absorption due to TDS plus a further absorption with a mean free path of 1800 Å have been included in the calculation. (b) Theoretical cross sections calculated with no absorption and with absorption due to TDS only are compared with the theoretical curve and experimental results in (a).

IV. CONCLUSIONS

The above method of calculating the cross section for K-shell ionization from first principles allows quantitative calculation of x-ray emission yields in crystals under dynamical diffraction conditions, accounting for both dechanneling effects (giving rise to a kinematical background) and interaction delocalization (convoluted with thermal motion of atoms). This has many implications for analysis of impurity site distributions (ALCHEMI), where the assumption that the cross section is proportional to the probability density of the incident electron has been used to date.[2] Once a fast electron has been thermally scattered (or involved in another wide angle inelastic event), integration over all angles to a good approximation yields a kinematic contribution to the characteristic x-ray count.

The assumption of a δ-function interaction for ionization for threshold energies in excess of 2 keV is reasonable given that thermal motions lead to an effective delocalization, with the thermal absorptive potential located on each atom with a half-width of about three times the projected rms displacement.[1] For lower energy excitations however the ionization delocalization may exceed the delocalization of the thermal absorptive potential. Similar conclusions were reached[27] in earlier investigations on the effects of ionization delocalization. The most important consideration in determining the degree of asymmetry or absolute changes in emission ratios with orientation is the inclusion of the kinematical background excitations to the dynamical response, with K-shell interaction delocalization being a relatively minor consideration for excitations above 2 keV.

Standard statistical multivariate methods[2] can be used for ALCHEMI analysis when impurities reside on host atom sites to reveal site distributions of the impurity in the host lattice. However for the case where impurities reside on interstitial sites or on light element sites which yield delocalized x-ray fluorescence the methods in this paper need to be employed. Krishnan, Rez, and Thomas[28] have investigated the applicability of the δ-function approximation to predict ALCHEMI responses from thin crystals of garnet.

If the final state of the scattered electron is detected or apertured down to a defined maximum scattering angle θ_{max}, higher energy incident electrons can lead to a more delocalized interaction as observed by EELS,[6] since smaller q channels exist for forward scattering, and delocalization will be a more important consideration than the case for x-ray emission where integration over all energies above the ionization threshold and all scattering angles occurs. For EELS diffraction of the ejected electron also needs to be taken into account. An expression for the cross section for an $(e,2e)$ event where channeling is included for all three electron is given in Ref. 18 and that result coupled with the work in this paper allows realistic calculation of both EELS and $(e,2e)$ cross sections from first principles.

ACKNOWLEDGMENTS

One of us (L.J.A.) acknowledges financial support from the Australian Research Council. We are grateful to Peter Miller (CSIRO Division of Materials Science and Technology) for assistance and advice.

[1] L. J. Allen and C. J. Rossouw, Phys. Rev. B **42**, 11 644 (1990).
[2] P. S. Turner, T. J. White, A. J. O'Connor, and C. J. Rossouw, J. Microscopy **162**, 369 (1990).
[3] R. F. Egerton, Ultramicroscopy **4**, 169 (1979).
[4] V. W. Maslen and C. J. Rossouw, Philos. Mag. A **47**, 119 (1983).
[5] V. W. Maslen and C. J. Rossouw, Philos. Mag. A **49**, 735 (1984).
[6] C. J. Rossouw and V. W. Maslen, Philos. Mag. A **49**, 743 (1984).
[7] S. J. Pennycook and J. Narayan, Phys. Rev. Lett. **54**, 1543 (1985).
[8] A. von Hugo, H. Kohl, and H. Rose, Optik **79**, 19 (1988).
[9] J. C. H. Spence, M. Kuwabara, and Y. Kim, Ultramicroscopy **26**, 103 (1988).
[10] V. W. Maslen, J. Phys. B **16**, 2065 (1983).
[11] C. J. Rossouw and V. W. Maslen, Ultramicroscopy **21**, 277 (1987).
[12] H. A. Bethe, Ann. Phys. (Leipzig) **87**, 55 (1928).
[13] L. J. Allen and C. J. Rossouw, Phys. Rev. B **39**, 8313 (1989).
[14] D. M. Bird and Q. A. King, Acta Crystallogr. Sect. A **46**, 202 (1990).
[15] D. M. Bird, Acta Crystallogr. Sect. A **46**, 208 (1990).
[16] R. D. Heidenreich, J. Appl. Phys. **33**, 2321 (1962).
[17] D. Cherns, A. Howie, and M. H. Jacobs, Z. Naturforsch. **28a**, 565 (1973).
[18] L. J. Allen, I. E. McCarthy, V. W. Maslen, and C. J. Rossouw, Aust. J. Phys. **43**, 453 (1990).
[19] J. S. Reid, Acta Crystallogr. Sect. A **39**, 1 (1983).
[20] J. C. H. Spence and J. Taftø, in *Scanning Electron Microscopy,* edited by O. Jahari (SEM Inc., Chicago, 1982), p. 523.
[21] J. Taftø, Phys. Rev. Lett. **51**, 654 (1983).
[22] J. Taftø, Z. Naturforsch. **34a**, 452 (1979).
[23] F. Glas and P. Hénoc, Philos. Mag. A **56**, 311 (1987).
[24] F. Glas, Ultramicroscopy **28**, 61 (1989).
[25] S. J. B. Reed, *Electron Microprobe Analysis* (Cambridge University Press, Cambridge, England, 1975).
[26] P. A. Doyle, Acta Crystallogr. Sect. A **26**, 133 (1970).
[27] A. J. Bourdillon, P. G. Self, and W. M. Stobbs, Philos. Mag. A **44**, 1335 (1981).
[28] K. M. Krishnan, P. Rez, and G. Thomas, Acta Crystallogr. Sect. B **41**, 396 (1985).